pubs.acs.org/journal/apchd5 Article

Schottky-Contacted WSe_2 Hot-Electron Photodetectors with Fast Response and High Sensitivity

Mingliang Zhang, Xingqiang Liu,* Xinpei Duan, Sen Zhang, Chang Liu, Da Wan, Guoli Li, Zhen Xia, Zhiyong Fan, and Lei Liao*

Cite This: *ACS Photonics* 2022, 9, 132−137

Read Online

ACCESS | Metrics & More | Article Recommendations | Supporting Information

ABSTRACT: Utilizing the short lifetime of hot electrons, ultrasensitive hot-electron photodetectors with fast response speed can be developed that have the potential to carve a niche among the photoconductive devices. Herein, high-performance WSe_2 photodetectors are fabricated based on hot-electron transportation, in which an ultrathin Al_2O_3 layer enables screening of high-energy hot electrons and promises ultrasensitive response to incident light, and the built-in electric field in Schottky junctions separates the photoinduced carriers for fast transient recovery. The hot-electron photodetectors demonstrated a high rectification ratio of 10^7 and an extremely low dark current of 1 pA/μm with a high I_{light}/I_{dark} ratio of 1.8×10^6. Moreover, a high responsivity of 3.69 A/W and detectivity of 2.39×10^{13} Jones at an incident light power of 5.0 $\mu W/cm^2$ are simultaneously achieved. The present strategy offers an alternative route for ultrasensitive photodetectors with fast response.

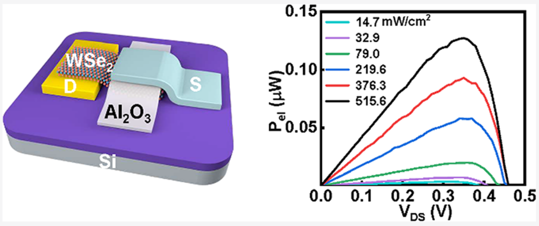

KEYWORDS: *hot-electron, tunneling, Schottky contact, built-in field, photodetector*

■ INTRODUCTION

Low-power photodetectors with fast response and high sensitivity are urgent for both scientific and industrial applications.[1−3] Two-dimensional (2D) materials show potential as channel materials in optoelectronic devices due to their strong interaction with incident light.[4−6] However, 2D material-based photodetectors typically exhibit low response speed and persistent current because of unintentionally introduced traps in ultrathin 2D channels as well as the long lifetime of trapped carriers.[7−9] To address these issues for ultrasensitive and fast-response applications, photoinduced carriers should be efficiently separated and thereafter collected by rationally designing the device structure. Hot electrons can be excited in metal by photon absorption with energy above the Fermi level of metal, which is beneficial for fabricating photodetectors. Hot-electron photodetectors (HEPs) rely on photoinjected hot electrons excited through photon absorption and extracted via internal photoemission with the intriguing prospect of direct below-bandgap photodetection.[8,10] It is worth pointing out that the lifetime of hot electrons is extremely short, wherein the thermal relaxation processes are accomplished in less than several picoseconds. In this case, hot electrons should be collected or extracted (i.e., charge transfer) on the same timescale before they lose their excess energy. The built-in field in Schottky junctions could efficiently separate the photoinduced electron−hole pairs. Therefore, hot-carrier photodetectors with Schottky contact can offer ultrasensitive and fast detection of incident light. Also, the hot electrons injected from the metal into an adjacent semiconductor across a tunneling barrier can further reduce the dark current. In addition, monochromatic hot electrons with high kinetic energy traverse across the energy barrier, creating a photocurrent that enables the detection of incident light with energy below the bandgap of semiconductors. Therefore, HEPs can afford ultrahigh sensitivity under weak incident light with wide detective spectral regions.

In this work, ultrasensitive fast-response WSe_2 HEPs with Schottky contact are demonstrated. Benefiting from the ultrathin thickness (5 nm) of the Al_2O_3 insulating layer, the dark current is suppressed by the barrier at the $Cr/Al_2O_3/WSe_2$ junction.[11] Under light illumination, the photocurrent is generated by the photoinduced carriers across the Al_2O_3 tunneling layer. The emission energy of hot electrons is observably increased, and the carrier transport time is greatly reduced.[8] Electrical transport measurements indicate a high rectification ratio of 10^7. A high photoresponsivity (R) of 3.69 A/W, high detectivity (D^*) of 2.39×10^{13} Jones at an incident light power density (P_{light}) of 5.0 $\mu W/cm^2$, and an I_{light}/I_{dark} ratio of 1.8×10^6 are obtained in the WSe_2 HEPs.

Received: August 18, 2021
Published: December 20, 2021

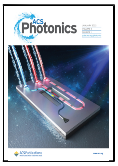

https://doi.org/10.1021/acsphotonics.1c01256
ACS Photonics 2022, 9, 132−137

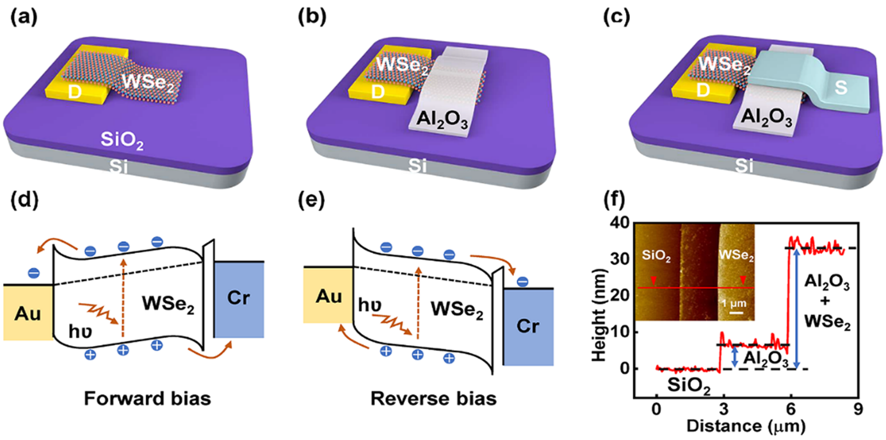

Figure 1. Schematic images of the WSe$_2$ hot-electron photodetectors (HEPs). (a−c) Fabrication processes of WSe$_2$ HEPs. (d) Band alignment of the device under forward bias. (e) Band diagram of the device under reverse bias. (f) Height profile across the WSe$_2$ HEPs and the inset is the AFM image.

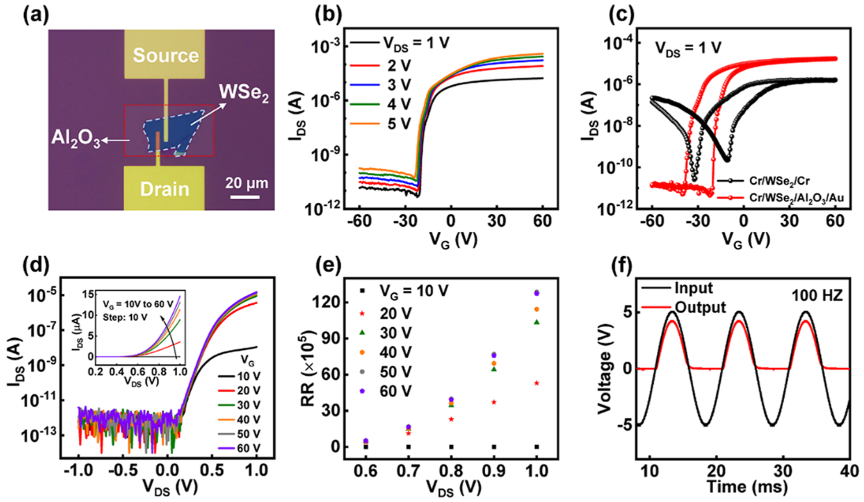

Figure 2. Electrical performance of the WSe$_2$ hot-electron diodes. (a) Optical image of the WSe$_2$ hot-electron diodes. The scale bar is 20 μm. The width and length of the devices are 2.3 and 2 μm, respectively. (b) Transfer characteristics of WSe$_2$ hot-electron devices. (c) Transfer curve comparison of the multilayer WSe$_2$ transistors with different contacts. (d) Output characteristics of WSe$_2$ hot-electron device at various gate voltages. The corresponding linear plots are shown in the inset. (e) Extracted currents RR in the dark as a function of V_{DS}. (f) Output voltage waveform obtained from an input sine waveform at 100 Hz.

■ RESULTS AND DISCUSSION

Figure 1a−c shows the schematic illustrating the fabrication of the WSe$_2$ hot-electron device with asymmetric contact. First, Cr/Au (15 nm/50 nm) electrodes are defined on a silicon substrate (with 300 nm SiO$_2$) by photolithography, and then metal evaporation and lift-off processes are introduced. WSe$_2$ flakes are obtained by mechanical exfoliation with Scotch tape[12] and then transferred onto the Au electrode to form ideal Schottky contact without the pinning effect.[13] Subsequently, a 5 nm Al$_2$O$_3$ tunneling layer is grown by atomic layer deposition. The top electrode region is patterned by e-beam lithography (EBL), and thermal evaporation is used to deposit Cr/Au (15 nm/50 nm) electrodes. The band alignment of WSe$_2$ hot-electron devices is shown in Figure 1d under forward bias. The ultrathin Al$_2$O$_3$ dielectric acts as the tunneling layer for carrier injection and screens the homochromous high-energy hot electrons.[14] Under forward bias, the Au/WSe$_2$ Schottky barrier height is reduced, leading to high photocurrent.[15] Figure 1e shows the band diagram under reverse bias. In this case, the depletion width of the Schottky barrier is significantly enlarged. By inserting an Al$_2$O$_3$ insulating layer, reverse leakage current is highly suppressed as well. Under reverse-biased conditions, the strength of the net electric-field of the device is enhanced, which comparatively accelerate the separation of photoinduced carriers. Atomic force microscopy (AFM) is employed to measure the height profile information, as shown in Figure 1f and the inset, which indicates the height profile across the WSe$_2$ hot-electron devices.

Figure 2a is the optical image of the WSe$_2$ hot-electron diodes. Transfer curves of the WSe$_2$ HEPs are provided in Figure 2b, indicating obvious n-type on−off characteristics. Metal/semiconductor contact is critical for optical and electrical characteristics of Schottky diodes.[16,17] Figure 2c is the transfer characteristic of the obtained WSe$_2$ hot-electron transistors with different contact types. Conventional multilayer WSe$_2$ transistors with thermally evaporated Cr/Au (15 nm/50 nm) (Cr/WSe$_2$/Cr) have ambipolar characteristics, which can be attributed to the Fermi pinning effect.[18,19] The tunneling layer and transferred van der Waals Au contact (Au/WSe$_2$/Al$_2$O$_3$/Cr) afford an obvious n-type characteristic in this

https://doi.org/10.1021/acsphotonics.1c01256
ACS Photonics 2022, 9, 132−137

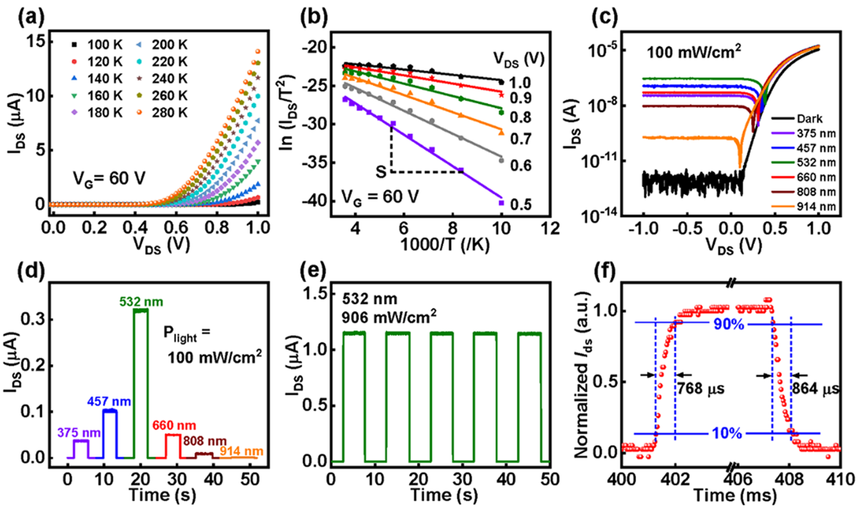

Figure 3. Temperature-dependent performance and photoresponse of the WSe$_2$ HEPs. (a) Output characteristics of WSe$_2$ HEPs at different temperatures. (b) Arrhenius plot ln (I_{DS}/T^2) versus 1000/T of the WSe$_2$ HEPs. (c) I_{DS}−V_{DS} curves under different incident light illuminations. (d) Photoresponse of the WSe$_2$ HEPs with different wavelengths. (e) Time-dependent dynamic photoresponse under 532 nm incident light illumination with a power intensity of 906 mW/cm^2. (f) High-resolution photoresponse indicates τ_{rise} and τ_{decay} values.

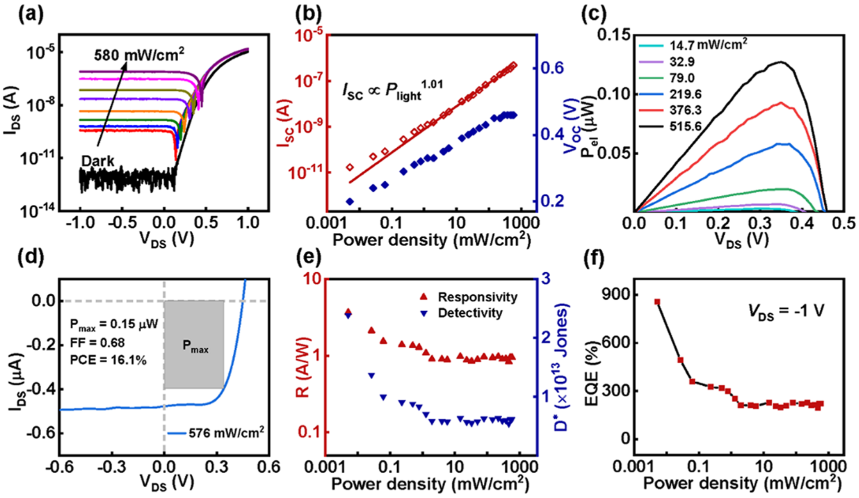

Figure 4. Illumination power-dependent photoresponse. (a) I_{DS}−V_{DS} characteristics of the WSe$_2$ HEPs under 532 nm laser illumination. (b) Short-circuit current (I_{SC}) and open-circuit voltage (V_{OC}) versus P_{light}. (c) Output electrical power P_{el} versus V_{DS}. (d) Output characteristic of the HEPs under light illumination. (e) Power-dependent photoresponsivity and detectivity. (f) External quantum efficiency of the WSe$_2$ hot-electron photodetector at V_{DS} = −1 V.

work. Figure 2d indicates the superior rectification ratio (RR) of 10^7, which is beyond the previously reported WSe$_2$-based diode.[20,21] Moreover, the reverse leakage current is significantly suppressed by the Schottky junctions and tunneling layer. The output current (I_{DS}) is plotted in Figure 2d. Figure 2e reveals the gate-dependent RR in the dark as a function of V_{DS}. The WSe$_2$ hot-electron diode exhibits an ideality factor (n) of 1.17 (Figure S1). The dynamic rectifying characteristics are shown in Figure 2f. An evident rectified output signal is traced by a digital oscilloscope with a 100 Hz input sine waveform of a peak-to-peak value of 10 V. There is little distortion and slight voltage drop (5 V down to 4.28 V) in the output waveform. Moreover, the WSe$_2$ hot-electron diode can still normally work under a wide range of frequencies, which makes it highly promising for primary element application in 2D material-based nanoelectronics.

Figure 3a shows the output characteristics at V_G = 60 V with temperatures ranging from 100 to 280 K. According to the traditional thermionic theory,[22−24] as shown below

$$I_{DS} = AA^*T^2\exp\left[-\frac{q}{k_BT}\left(\varphi_B - \frac{V_{DS}}{n}\right)\right]$$

where A is the area of the photodetector, A^* is the Richardson's constant, q is the elementary electron charge, k_B is the Boltzmann constant, T is the temperature, V_{DS} is the applied source-drain bias, and n is the ideality factor. Obviously, the on-state current increases with temperature, indicating that the thermionic emission over Schottky barrier (SB) increases with current flowing. Therefore, the dominant tunnel transport is assisted by thermionic emission.[25,26] Figure 3b shows the gate-dependent Arrhenius plot of the WSe$_2$ HEPs, and the calculated total barrier height of the Au/WSe$_2$/Al$_2$O$_3$/Cr is about 307 meV at V_G = 60 V, as shown in Figure

S2. Also, the corresponding band alignment of the HEPs with different gate bias values under light illumination is shown in Figure S3. Figure 3c is the linear output plots of the WSe_2 HEPs at V_G = 60 V under illumination. The photocurrent reached the peak value with 532 nm incident light illumination (Figure 3d), which is measured with a P_{light} of 100 mW/cm^2. Moreover, the on−off characteristics of WSe_2 HEPs are shown in Figure 3e, where the device exhibits reliable and fast on−off switching performance. Figure 3f is the high-resolution photoresponse of the HEPs, and the response (τ_{rise}) and recover (τ_{decay}) times are 768 and 864 μs, respectively. Since the Al_2O_3 tunneling barrier can screen monochromatic hot electrons with high kinetic energy, the built-in electric field in the SB contact region further affords the short response of the WSe_2 HEPs, as shown in Figure S4. Therefore, the WSe_2 HEPs present superior speed among the previously reported 2D material-based photodetectors.[27,28]

The power-dependent photoresponse is measured to state the photoelectric effect of Schottky-contacted WSe_2 HEPs. Figure 4a indicates that the photocurrent obviously increases with P_{light}. The photoinduced carriers are generated and then transported through the ultrathin Al_2O_3 tunneling layer.[29] At an incident light power of 580 mW/cm^2, the I_{light}/I_{dark} ratio is 1.8×10^6. The large I_{light}/I_{dark} value is ascribed to the thermally distributed hot carriers. In the previously reported work, photoinduced carriers were generated near the Au/WSe_2 junction region.[15] The photoinduced carriers are recombined through the WSe_2 layer, and thus, the previous reported works present low photoresponsivity and long response time. In contrast, the vertical heterostructure in this work broadens the carrier distribution region, leading to a high I_{light}/I_{dark} ratio. In Figure 4b, the short current (I_{SC}) and open-circuit voltage (V_{OC}) simultaneously increase with P_{light}. By fitting as $I_{SC} = AP_{light}{}^{\theta}$, the HEPs present an ideal θ value of 1.01, indicating the high quality of the interfaces.[30,31] Figure 4c is the output electrical power (P_{el}) versus V_{DS} with varied incident light density. With a continuous shift of I_{DS}−V_{DS} characteristics, the peak P_{el} is increased with P_{light}. The maximum output of electrical power (P_{max}) is indicated in Figure 4d, and a typical P_{max} = 0.15 μW is obtained. Also, the fill factor (FF) and power conversion efficiency (PCE) are 0.68 and 16.1%, which are obtained with P_{light} = 576 mW/cm^2, respectively. Figure S5 is the power-dependent FF and PCE, and both FF and PCE decrease with P_{light}. As shown in Figure 4e, both R and D^* decrease with P_{light}. Based on the measured low-frequency noise in Figure S6, a high R of 3.69 A/W and D^* of 2.39×10^{13} Jones are simultaneously obtained at an ultralow P_{light} = 5.0 μW/cm^2, which is superior to those of the previously reported works.[32−34] Although the scattering of photoinduced electrons would degrade the responsivity with high incident power, due to the dominant hot electron transformation mechanism of the photodetectors, negligible changes of responsivity are observed when P_{light} is above 1 mW/cm^2, which is superior to previously reported devices.[35,36] As shown in Figure S7, the HEPs present a high signal-to-noise ratio above 10^5 as well as desirable linear dynamic range (LDR) values. The external quantum efficiency (EQE) decreases with P_{light} and reaches a peak value of 859%, as shown in Figure 4f. The built-in field in Schottky junctions facilitates the injected photoinduced electron transportation in WSe_2, and the applied voltage pulls out the electrons in WSe_2, leading to an increased photocurrent, and this affords the high EQE. Photogain (G) is calculated to be 5.8, which further indicates that the photoinduced carriers circulate several times before recombination.

CONCLUSIONS

In summary, Schottky-contacted WSe_2 HEPs with ultrahigh sensitivity and fast response are developed. The hot electrons promise ultrasensitive response to incident light, and the built-in electric field in Schottky barriers at the contact region spontaneously and rapidly separates the photoinduced carriers before they lose their excess energy. Therefore, the photodetectors present fast response speed even under weak incident light. Photoinduced hot electrons in WSe_2 are transported by tunneling, leading to a high rectification ratio. Also, the reverse leakage current is suppressed to 1 pA/μm by the large depletion region width of the Schottky barrier. This work presents an alternative strategy for developing ultrasensitive and fast future electronic and optoelectronic devices.

METHODS

Device Fabrication. Cr/Au electrodes were deposited on a silicon substrate with a 300 nm SiO_2 layer using conventional photolithography followed by thermal evaporation. Then, WSe_2 flakes were peeled with Scotch tape and transferred onto a Cr/Au electrode to form ideal Schottky contact without the pinning effect. After that, a 5 nm Al_2O_3 tunneling layer was grown by atomic layer deposition (ALD). The growth rate is 1.0 Å per cycle as follows: Trimethylaluminum (TMA) is used as a precursor source, while the H_2O source was kept at room temperature. The flow rate of the Ar carrier gas was 50 sccm. The pulse times for TMA and H_2O are 0.1 and 0.4 s, and the post-purge times are 12 and 18 s, respectively; subsequently, the copolymer (MMA) was spin-coated at a speed of 3000 rpm and baked on a hot plate at 150 °C for 1 min, and then polymethyl methacrylate (PMMA, 495k) was spin-coated at 3000 rpm and baked at 150 °C for 5 min. Finally, the top Cr/Au (15 nm/50 nm) electrode was fabricated by EBL, e-beam evaporation, and lift-off processes.

Material Characterization and Device Measurement. Optical images were obtained by an Olympus BX53, and the thickness of Al_2O_3 and WSe_2 with the corresponding AFM image was obtained on a Park XE7. EBL was carried out on a Raith pattern generator and SEM combination. Electrical measurements were carried out by employing a Lake Shore TTPX probe station and Agilent B1500A semiconductor parameter analyzer. The light sources were lasers with wavelengths of 375, 457, 532, 660, 808, and 914 nm, respectively.

ASSOCIATED CONTENT

Supporting Information

The Supporting Information is available free of charge at https://pubs.acs.org/doi/10.1021/acsphotonics.1c01256.

Ideality factor of the WSe_2 diode; extracted SB height of the hot-electron device; band diagram of the WSe_2 hot-electron diode under different gate voltages; comparison of the rectification behavior and photoresponse without and with the Al_2O_3 layer; light power-dependent FF and PCE; low-frequency noise of the hot-electron devices; and extracted SNR and LDR values of the WSe_2 hot-electron photodetectors (PDF)

AUTHOR INFORMATION

Corresponding Authors

Xingqiang Liu – *Key Laboratory for Micro/Nano Optoelectronic Devices of Ministry of Education & Hunan Provincial Key Laboratory of Low-Dimensional Structural Physics and Devices, School of Physics and Electronics, Hunan University, Changsha 410082, China;* orcid.org/0000-0002-3598-8755; Email: liuxq@hnu.edu.cn

Lei Liao – *Key Laboratory for Micro/Nano Optoelectronic Devices of Ministry of Education & Hunan Provincial Key Laboratory of Low-Dimensional Structural Physics and Devices, School of Physics and Electronics, Hunan University, Changsha 410082, China;* orcid.org/0000-0003-1325-2410; Email: liaolei@whu.edu.cn

Authors

Mingliang Zhang – *Key Laboratory for Micro/Nano Optoelectronic Devices of Ministry of Education & Hunan Provincial Key Laboratory of Low-Dimensional Structural Physics and Devices, School of Physics and Electronics, Hunan University, Changsha 410082, China*

Xinpei Duan – *Key Laboratory for Micro/Nano Optoelectronic Devices of Ministry of Education & Hunan Provincial Key Laboratory of Low-Dimensional Structural Physics and Devices, School of Physics and Electronics, Hunan University, Changsha 410082, China*

Sen Zhang – *Key Laboratory for Micro/Nano Optoelectronic Devices of Ministry of Education & Hunan Provincial Key Laboratory of Low-Dimensional Structural Physics and Devices, School of Physics and Electronics, Hunan University, Changsha 410082, China*

Chang Liu – *Key Laboratory for Micro/Nano Optoelectronic Devices of Ministry of Education & Hunan Provincial Key Laboratory of Low-Dimensional Structural Physics and Devices, School of Physics and Electronics, Hunan University, Changsha 410082, China*

Da Wan – *School of Information Science and Engineering, Wuhan University of Science and Technology, Wuhan 430081, China*

Guoli Li – *Key Laboratory for Micro/Nano Optoelectronic Devices of Ministry of Education & Hunan Provincial Key Laboratory of Low-Dimensional Structural Physics and Devices, School of Physics and Electronics, Hunan University, Changsha 410082, China*

Zhen Xia – *Key Laboratory for Micro/Nano Optoelectronic Devices of Ministry of Education & Hunan Provincial Key Laboratory of Low-Dimensional Structural Physics and Devices, School of Physics and Electronics, Hunan University, Changsha 410082, China*

Zhiyong Fan – *Department of Electronic & Computer Engineering, Hong Kong University of Science & Technology, Hong Kong SAR 999077, China;* orcid.org/0000-0002-5397-0129

Complete contact information is available at: https://pubs.acs.org/10.1021/acsphotonics.1c01256

Author Contributions

L.L. and X.L. conceived and designed the experiments. M.Z. and X.D. prepared the samples and finished related tests and data analysis. M.Z. and X.L. wrote the manuscript. S.Z. and C.L. finished the 3D drawing design. D.W., G.L., Z.X., and Z.F. present the suggestions for improving the quality of this work and revised the manuscript. Related tests and result analysis were done by M.Z. using protocols provided by L.L. All authors examined and commented on the manuscript.

Notes

The authors declare no competing financial interest.

ACKNOWLEDGMENTS

This work was supported by the National Key Research and Development Program of Ministry of Science and Technology (no. 2018YFA0703700), China National Funds for Distinguished Young Scientists Grant 61925403, the National Natural Science Foundation of China (grant nos. 61851403 and 51872084), Natural Science Foundation of Hunan Province (grant nos. 2020JJ1002 and 2021JJ20028), and partly by the Key Research and Development Plan of Hunan Province under grant nos. 2022WK2001 and 2018GK2064.

REFERENCES

(1) Long, M.; Wang, P.; Fang, H.; Hu, W. Progress, Challenges, and Opportunities for 2D Material Based Photodetectors. *Adv. Funct. Mater.* **2019**, *29*, 1803807.

(2) Lopez-Sanchez, O.; Lembke, D.; Kayci, M.; Radenovic, A.; Kis, A. Ultrasensitive Photodetectors Based on Monolayer MoS_2. *Nat. Nanotechnol.* **2013**, *8*, 497–501.

(3) Ren, H.; Liu, Y.; Zhang, L.; Liu, K. Synthesis, Properties, and Applications of Large-Scale Two-Dimensional Materials by Polymer-Assisted Deposition. *J. Semicond.* **2019**, *40*, No. 061003.

(4) Zhang, W.; Huang, J. K.; Chen, C. H.; Chang, Y. H.; Cheng, Y. J.; Li, L. J. High-Gain Phototransistors Based on a CVD MoS_2 Monolayer. *Adv. Mater.* **2013**, *25*, 3456–3461.

(5) Wang, X.; Wang, P.; Wang, J.; Hu, W.; Zhou, X.; Guo, N.; Huang, H.; Sun, S.; Shen, H.; Lin, T.; Tang, M.; Liao, L.; Jiang, A.; Sun, J.; Meng, X.; Chen, X.; Lu, W.; Chu, J. Ultrasensitive and Broadband MoS_2 Photodetector Driven by Ferroelectrics. *Adv. Mater.* **2015**, *27*, 6575–6581.

(6) Liu, R.; Wang, F.; Liu, L.; He, X.; Chen, J.; Li, Y.; Zhai, T. Band Alignment Engineering in Two-Dimensional Transition Metal Dichalcogenide-Based Heterostructures for Photodetectors. *Small Struct.* **2020**, *2*, 2000136.

(7) Mueller, T.; Xia, F.; Avouris, P. Graphene Photodetectors for High-Speed Optical Communications. *Nat. Photonics* **2010**, *4*, 297–301.

(8) Sun, D.; Aivazian, G.; Jones, A. M.; Ross, J. S.; Yao, W.; Cobden, D.; Xu, X. Ultrafast Hot-Carrier-Dominated Photocurrent in Graphene. *Nat. Nanotechnol.* **2012**, *7*, 114–118.

(9) Xia, F.; Mueller, T.; Lin, Y. M.; Valdes-Garcia, A.; Avouris, P. Ultrafast Graphene Photodetector. *Nat. Nanotechnol.* **2009**, *4*, 839–843.

(10) Kim, Y. R.; Phan, T. L.; Shin, Y. S.; Kang, W. T.; Won, U. Y.; Lee, I.; Kim, J. E.; Kim, K.; Lee, Y. H.; Yu, W. J. Unveiling the Hot Carrier Distribution in Vertical Graphene/h-BN/Au Van der Waals Heterostructures for High-Performance Photodetector. *ACS Appl. Mater. Interfaces* **2020**, *12*, 10772–10780.

(11) Gao, F.; Chen, H.; Feng, W.; Hu, Y.; Shang, H.; Xu, B.; Zhang, J.; Xu, C. Y.; Hu, P. High-Performance Van der Waals Metal-Insulator-Semiconductor Photodetector Optimized with Valence Band Matching. *Adv. Funct. Mater.* **2021**, *31*, 2104359.

(12) Zhang, X.; Li, Y.; Mu, W.; Bai, W.; Sun, X.; Zhao, M.; Zhang, Z.; Shan, F.; Yang, Z. Advanced Tape-Exfoliated Method for Preparing Large-Area 2D Monolayers: a Review. *2D Mater.* **2021**, *8*, No. 032002.

(13) Kong, L.; Zhang, X.; Tao, Q.; Zhang, M.; Dang, W.; Li, Z.; Feng, L.; Liao, L.; Duan, X.; Liu, Y. Doping-Free Complementary WSe_2 Circuit via Van der Waals Metal Integration. *Nat. Commun.* **2020**, *11*, 1866.

(14) Vu, Q. A.; Lee, J. H.; Nguyen, V. L.; Shin, Y. S.; Lim, S. C.; Lee, K.; Heo, J.; Park, S.; Kim, K.; Lee, Y. H.; Yu, W. J. Tuning Carrier

Tunneling in Van der Waals Heterostructures for Ultrahigh Detectivity. *Nano Lett.* **2017**, *17*, 453−459.

(15) Luo, M.; Wu, F.; Long, M.; Chen, X. WSe_2/Au Vertical Schottky Junction Photodetector With Low Dark Current and Fast Photoresponse. *Nanotechnology* **2018**, *29*, 444001.

(16) Liu, Y.; Guo, J.; Zhu, E.; Liao, L.; Lee, S. J.; Ding, M.; Shakir, I.; Gambin, V.; Huang, Y.; Duan, X. Approaching the Schottky-Mott Limit in Van der Waals Metal−Semiconductor Junctions. *Nature* **2018**, *557*, 696−700.

(17) Tan, J.; Li, S.; Liu, B.; Cheng, H.-M. Structure, Preparation, and Applications of 2D Material-Based Metal-Semiconductor Heterostructures. *Small Struct.* **2020**, *2*, 2000093.

(18) Podzorov, V.; Gershenson, M. E.; Kloc, C.; Zeis, R.; Bucher, E. High-Mobility Field-Effect Transistors Based on Transition Metal Dichalcogenides. *Appl. Phys. Lett.* **2004**, *84*, 3301−3303.

(19) Zhou, C.; Zhao, Y.; Raju, S.; Wang, Y.; Lin, Z.; Chan, M.; Chai, Y. Carrier Type Control of WSe_2 Field-Effect Transistors by Thickness Modulation and MoO_3 Layer Doping. *Adv. Funct. Mater.* **2016**, *26*, 4223−4230.

(20) Tosun, M.; Chuang, S.; Fang, H.; Sachid, A. B.; Hettick, M.; Lin, Y.; Zeng, Y.; Javey, A. High-Gain Inverters Based on WSe_2 Complementary Field-Effect Transistors. *ACS Nano* **2014**, *8*, 4948−4953.

(21) Cheng, R.; Li, D.; Zhou, H.; Wang, C.; Yin, A.; Jiang, S.; Liu, Y.; Chen, Y.; Huang, Y.; Duan, X. Electroluminescence and Photocurrent Generation from Atomically Sharp WSe_2/MoS_2 Heterojunction p-n Diodes. *Nano Lett.* **2014**, *14*, 5590−5597.

(22) Dankert, A.; Langouche, L.; Kamalakar, M. V.; Dash, S. P. High-Performance Molybdenum Disulfide Field-Effect Transistors with Spin Tunnel Contacts. *ACS Nano* **2014**, *8*, 476−482.

(23) Kamalakar, M. V.; Madhushankar, B. N.; Dankert, A.; Dash, S. P. Low Schottky Barrier Black Phosphorus Field-Effect Devices with Ferromagnetic Tunnel Contacts. *Small* **2015**, *11*, 2209−2216.

(24) Yu, W. J.; Li, Z.; Zhou, H.; Chen, Y.; Wang, Y.; Huang, Y.; Duan, X. Vertically Stacked Multi-Heterostructures of Layered Materials for Logic Transistors and Complementary Inverters. *Nat. Mater.* **2013**, *12*, 246−252.

(25) Pande, G.; Siao, J. Y.; Chen, W. L.; Lee, C. J.; Sankar, R.; Chang, Y. M.; Chen, C. D.; Chang, W. H.; Chou, F. C.; Lin, M. T. Ultralow Schottky Barriers in Hexagonal Boron Nitride-Encapsulated Monolayer WSe_2 Tunnel Field-Effect Transistors. *ACS Appl. Mater. Interfaces* **2020**, *12*, 18667−18673.

(26) Di Bartolomeo, A.; Grillo, A.; Urban, F.; Iemmo, L.; Giubileo, F.; Luongo, G.; Amato, G.; Croin, L.; Sun, L.; Liang, S.-J.; Ang, L. K. Asymmetric Schottky Contacts in Bilayer MoS_2 Field Effect Transistors. *Adv. Funct. Mater.* **2018**, *28*, 1800657.

(27) Zhang, W.; Chiu, M.-H.; Chen, C.-H.; Chen, W.; Li, L.-J.; Wee, A. T. S. Role of Metal Contacts in High-Performance Phototransistors Based on WSe_2 Monolayers. *ACS Nano* **2014**, *8*, 8653−8661.

(28) Tian, X.; Van der Liu, Y. Waals Heterojunction $ReSe_2$/WSe_2 Polarization-Resolved Photodetector. *J. Semicond.* **2021**, *42*, No. 032001.

(29) Xie, C.; Yan, F. Flexible Photodetectors Based on Novel Functional Materials. *Small* **2017**, *13*, 1701822.

(30) Ouyang, W.; Teng, F.; Fang, X. High Performance BiOCl Nanosheets/TiO_2 Nanotube Arrays Heterojunction UV Photodetector: The Influences of Self-Induced Inner Electric Fields in the BiOCl Nanosheets. *Adv. Funct. Mater.* **2018**, *28*, 1707178.

(31) Wang, L.; Huang, L.; Tan, W. C.; Feng, X.; Chen, L.; Huang, X.; Ang, K.-W. 2D Photovoltaic Devices: Progress and Prospects. *Small Methods* **2018**, *2*, 1700294.

(32) Kim, C. O.; Kim, S.; Shin, D. H.; Kang, S. S.; Kim, J. M.; Jang, C. W.; Joo, S. S.; Lee, J. S.; Kim, J. H.; Choi, S. H.; Hwang, E. High Photoresponsivity in an All-Graphene p−n Vertical Junction Photodetector. *Nat. Commun.* **2014**, *5*, 3249.

(33) Xue, Y.; Zhang, Y.; Liu, Y.; Liu, H.; Song, J.; Sophia, J.; Liu, J.; Xu, Z.; Xu, Q.; Wang, Z.; Zheng, J.; Liu, Y.; Li, S.; Bao, Q. Scalable Production of a Few-Layer MoS_2/WS_2 Vertical Heterojunction Array and Its Application for Photodetectors. *ACS Nano* **2016**, *10*, 573−580.

(34) Song, W.; Chen, J.; Li, Z.; Fang, X. Self-Powered MXene/GaN Van der Waals Heterojunction Ultraviolet Photodiodes with Superhigh Efficiency and Stable Current Outputs. *Adv. Mater.* **2021**, *33*, 2101059.

(35) Kang, D.-H.; Kim, M.-S.; Shim, J.; Jeon, J.; Park, H.-Y.; Jung, W.-S.; Yu, H.-Y.; Pang, C.-H.; Lee, S.; Park, J.-H. High-Performance Transition Metal Dichalcogenide Photodetectors Enhanced by Self-Assembled Monolayer Doping. *Adv. Funct. Mater.* **2015**, *25*, 4219−4227.

(36) Nguyen, D. A.; Oh, H. M.; Duong, N. T.; Bang, S.; Yoon, S. J.; Jeong, M. S. Highly Enhanced Photoresponsivity of a Monolayer WSe_2 Photodetector with Nitrogen-Doped Graphene Quantum Dots. *ACS Appl. Mater. Interfaces* **2018**, *10*, 10322−10329.